



**HAL**  
open science

## **Increased surface P2X4 receptor regulates anxiety and memory in 3 P2X4 internalization-defective knock-in mice**

Eléonore Bertin, Thomas Deluc, Estelle Toulmé, Kjara S Pilch, Audrey Martinez, Johan-Till Pougnet, Evelyne Doudnikoff, Anne-Emilie Allain, Philine Bergmann, Marion Rousseau, et al.

► **To cite this version:**

Eléonore Bertin, Thomas Deluc, Estelle Toulmé, Kjara S Pilch, Audrey Martinez, et al.. Increased surface P2X4 receptor regulates anxiety and memory in 3 P2X4 internalization-defective knock-in mice. *Molecular Psychiatry*, 2020, 10.1038/s41380-019-0641-8 . hal-03003954

**HAL Id: hal-03003954**

**<https://hal.science/hal-03003954>**

Submitted on 13 Nov 2020

**HAL** is a multi-disciplinary open access archive for the deposit and dissemination of scientific research documents, whether they are published or not. The documents may come from teaching and research institutions in France or abroad, or from public or private research centers.

L'archive ouverte pluridisciplinaire **HAL**, est destinée au dépôt et à la diffusion de documents scientifiques de niveau recherche, publiés ou non, émanant des établissements d'enseignement et de recherche français ou étrangers, des laboratoires publics ou privés.



# Increased surface P2X4 receptor regulates anxiety and memory in P2X4 internalization-defective knock-in mice

Eléonore Bertin<sup>1,2</sup> · Thomas Deluc<sup>1,2,3</sup> · Kjara S. Pilch<sup>1,2</sup> · Audrey Martinez<sup>1,2</sup> · Johan-Till Pougnet<sup>1,2</sup> · Evelyne Doudnikoff<sup>1,2</sup> · Anne-Emilie Allain<sup>4,5</sup> · Philine Bergmann<sup>6</sup> · Marion Rousseau<sup>7</sup> · Estelle Toulmé<sup>1,2</sup> · Erwan Bezard<sup>1,2</sup> · Friedrich Koch-Nolte<sup>6</sup> · Philippe Séguéla<sup>3</sup> · Sabine Lévi<sup>7</sup> · Bruno Bontempi<sup>1,2</sup> · François Georges<sup>1,2</sup> · Sandrine S. Bertrand<sup>4,5</sup> · Olivier Nicole<sup>1,2</sup> · Eric Boué-Grabot<sup>1,2</sup>

Received: 16 September 2019 / Revised: 10 December 2019 / Accepted: 12 December 2019  
© The Author(s), under exclusive licence to Springer Nature Limited 2020

## Abstract

ATP signaling and surface P2X4 receptors are upregulated selectively in neurons and/or glia in various CNS disorders including anxiety, chronic pain, epilepsy, ischemia, and neurodegenerative diseases. However, the cell-specific functions of P2X4 in pathological contexts remain elusive. To elucidate P2X4 functions, we created a conditional transgenic knock-in P2X4 mouse line (Floxed P2X4mCherryIN) allowing the Cre activity-dependent genetic swapping of the internalization motif of P2X4 by the fluorescent mCherry protein to prevent constitutive endocytosis of P2X4. By combining molecular, cellular, electrophysiological, and behavioral approaches, we characterized two distinct knock-in mouse lines expressing noninternalized P2X4mCherryIN either exclusively in excitatory forebrain neurons or in all cells natively expressing P2X4. The genetic substitution of wild-type P2X4 by noninternalized P2X4mCherryIN in both knock-in mouse models did not alter the sparse distribution and subcellular localization of P2X4 but increased the number of P2X4 receptors at the surface of the targeted cells mimicking the pathological increased surface P2X4 state. Increased surface P2X4 density in the hippocampus of knock-in mice altered LTP and LTD plasticity phenomena at CA1 synapses without affecting basal excitatory transmission. Moreover, these cellular events translated into anxiolytic effects and deficits in spatial memory. Our results show that increased surface density of neuronal P2X4 contributes to synaptic deficits and alterations in anxiety and memory functions consistent with the implication of P2X4 in neuropsychiatric and neurodegenerative disorders. Furthermore, these conditional P2X4mCherryIN knock-in mice will allow exploring the cell-specific roles of P2X4 in various physiological and pathological contexts.

These authors contributed equally: Eléonore Bertin, Thomas Deluc, Kjara S. Pilch

**Supplementary information** The online version of this article (<https://doi.org/10.1038/s41380-019-0641-8>) contains supplementary material, which is available to authorized users.

✉ Eric Boué-Grabot  
eric.boue-grabot@u-bordeaux.fr

- 1 Université de Bordeaux, Institut des Maladies Neurodégénératives, UMR 5293, F-33000 Bordeaux, France
- 2 CNRS, Institut des Maladies Neurodégénératives, UMR 5293, F-33000 Bordeaux, France
- 3 Department of Neurology and Neurosurgery, Montreal Neurological Institute, Alan Edwards Centre for Research on Pain, McGill University, Montreal, QC H3A 2B4, Canada

## Introduction

The release and extracellular action of ATP are a widespread mechanism for cell-to-cell communication in living organisms through activation of P2X and P2Y receptors expressed at the cell surface of most tissues, including the nervous system [1]. Several P2X receptors (P2X) are

- 4 Université de Bordeaux, Institut de Neurosciences Cognitives et Intégratives d'Aquitaine, UMR5287, F-33000 Bordeaux, France
- 5 CNRS, Institut de Neurosciences Cognitives et Intégratives d'Aquitaine, UMR5287, F-33000 Bordeaux, France
- 6 Institute of Immunology, University Medical Center Hamburg-Eppendorf, Martinistr. 52, D-20246 Hamburg, Germany
- 7 INSERM UMR-S 1270, Sorbonne Université, Institut du Fer à Moulin, 75005 Paris, France

expressed in the central nervous system (CNS) with varying distributions in neurons as well as in glia [2–4]. P2X receptors are ATP-gated cation channels and their activation by ATP, co-released by neurons with other neurotransmitters [5, 6] or released as a gliotransmitter by astrocytes [7–9], has profound modulatory actions at synapses [1, 10, 11]. Among the seven P2X subunits, P2X4 displays high calcium permeability [12, 13] and a widespread distribution in CNS neurons and glial cells as well as in peripheral tissues [14–16]. Nevertheless P2X4 expression in the brain is sparse [15] and its contribution to the synaptic modulation in normal conditions remains debated [17, 18]. A growing body of evidence suggests that upregulated P2X4 expression plays important roles in various CNS disorders including chronic pain and neurodegenerative diseases such as Alzheimer’s disease (AD) or amyotrophic lateral sclerosis (ALS) [19–26]. In the healthy organism, P2X4 is constitutively internalized by the interaction between the adapter protein 2 (AP2) and a noncanonical endocytosis motif in the C-tail of P2X4 subunit [27, 28]. As a result, P2X4 is found preferentially in intracellular compartments ensuring a low surface expression not only in neurons, but also in microglia and macrophages [29–32]. Intracellular P2X4 may promote vesicle fusion of endosomes or lysosomes [32, 33]. Importantly, intracellular P2X4 pools can be mobilized and trafficked to the cell surface [31, 34], consistent with the critical role of increased P2X4 surface expression in pathological states [19, 21, 24–26, 35–37]. The specific increase in P2X4 expression and surface trafficking in spinal microglia is critical for the pathogenesis of chronic pain [24, 38–41]. Increased P2X4 expression and surface density in neurons have been observed in the hippocampus or in the spinal cord of AD or ALS mouse models, respectively, suggesting that upregulated P2X4 may contribute to synaptic dysfunction and/or cell death in AD or ALS [23, 25, 26, 35]. However, the extent of the upregulated surface P2X4 state and the cell-specific functions of P2X4 in the pathological context remain elusive.

Here we report the development of conditional knock-in (P2X4mCherryIN) mice mimicking a pathological increase of surface P2X4. We show that the increase of P2X4 at the surface of excitatory neurons decreases anxiety, impairs memory processing, and alters activity-dependent synaptic plasticity phenomena in the hippocampus suggesting that upregulation of neuronal P2X4 observed in AD [25] may have key roles in AD pathogenesis. Overall, we provide an innovative knock-in P2X4 model to study the functional contributions of upregulated P2X4 in specific cells of the nervous system but also in peripheral tissues throughout the body.

## Materials and methods

### Experimental model

The *P2rx4* conditional knock-in mouse line was established at the MCI/ICS (Mouse Clinical Institute, France). *Xenopus* oocytes were isolated as described [42, 43]. Cultures of hippocampal neurons were prepared as described [44] with some modifications. Peritoneal cells were isolated as described [45] (see Supplementary information).

### Immunofluorescence and microscopy

Immunofluorescence studies of neurons, macrophages, brain immunohistochemistry, and image acquisition are described in the Supplementary and electron microscopy (E. M.) was performed as previously described [46] (see Supplementary information).

### Biotinylation assays and immunoblotting

Surface biotinylation experiments were performed as described previously [8, 43, 47] from injected *Xenopus* oocytes, mouse peritoneal macrophages, and hippocampal cell cultures (see Supplementary information).

### Electrophysiology

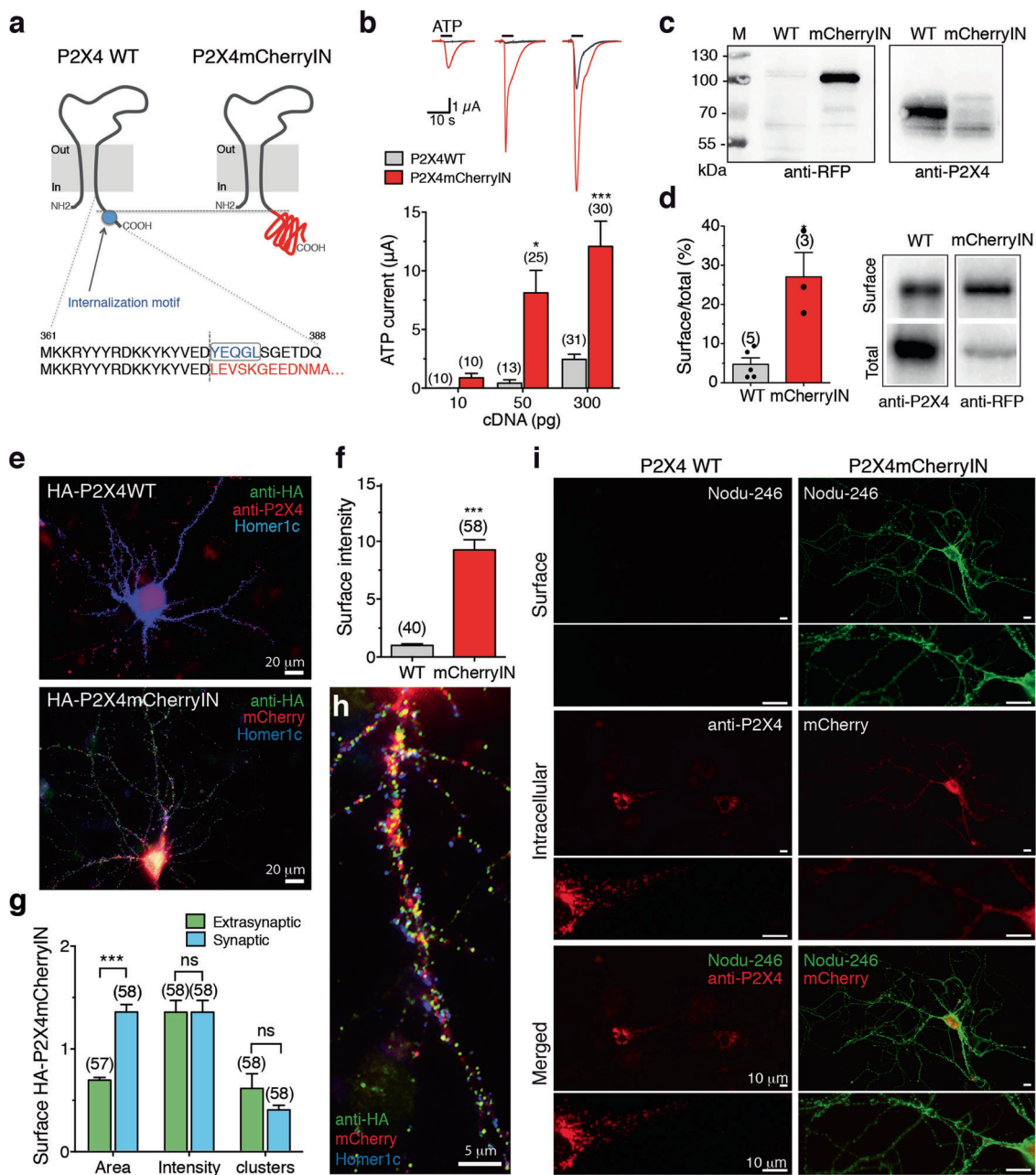
Extracellular field recordings and induction of synaptic plasticity in hippocampal brain slices are described in the Supplementary. Two-electrode voltage-clamp recordings from *Xenopus* oocyte were performed as previously described (see Supplementary information).

### Mouse behavior

Open field procedure, novel object recognition test [48, 49], elevated plus maze [50], the Y-maze two-trial procedure [51], and spatial memory testing conducted in an eight-arm radial maze are described in the Supplementary information.

### Quantification and statistical analysis

The number of independent experiments or animals ( $n$ ), the statistical test used for comparison and the statistical significance ( $p$  values) are specified for each figure panel in the corresponding figure legend. Data are presented as mean  $\pm$  s.e.m. Data were analyzed and graphs were generated using GraphPad Prism.



## Results

### Substitution of the internalization motif of P2X4 by mCherry protein increases surface density of functional P2X4 receptors

Mutation or ablation of the endocytosis motif of P2X4 (Y<sup>378</sup>xxGL) was previously shown to increase the surface trafficking of P2X4 without altering its functional properties [28, 43]. We generated a P2X4mCherryIN construct in which the endocytosis motif of mouse wild-type (WT) P2X4 was suppressed by swapping the last 11 amino acids in the C-tail of P2X4 with the sequence coding for the red

fluorescent protein mCherry (Fig. 1a). ATP-evoked currents recorded from P2X4WT or P2X4mCherryIN expressing *Xenopus* oocytes (Fig. 1b) showed that P2X4mCherryIN response amplitudes were significantly larger than those recorded from P2X4WT (Fig. 1b). We next examined the surface level of P2X4WT and P2X4mCherryIN by biotinylation assays and western blotting from oocytes (Fig. 1c, d). Anti-P2X4 antibodies allowed the detection of P2X4WT (70 kDa) but not P2X4mCherryIN (the anti-P2X4 epitope (amino acids 370–388) is deleted in P2X4mCherryIN constructs). P2X4mCherryIN was detected using anti-RFP antibodies showing a band at 100 kDa in agreement with the fusion of mCherry (30 kDa) to P2X4 (Fig. 1c). Surface/total

◀ **Fig. 1 Substitution of the internalization motif of P2X4 by mCherry increases ATP current density and surface expression of P2X4 receptors.** **a** Schematic representation of the mouse P2X4 subunit topology and C-terminal sequence of wild-type P2X4 (WT) and P2X4mCherryIN subunits. The AP2 binding site (blue circle) within the C-terminal sequence of mouse P2X4WT was exchanged for the red fluorescent protein mCherry sequence (P2X4) preventing clathrin-dependent internalization. **b** Representative superimposed currents evoked by applications of ATP (100  $\mu$ M, 5 s) from oocytes expressing wild-type P2X4 (WT) (black traces) or P2X4mCherryIN receptors (red traces). Bar graphs of the mean amplitude of ATP current recorded from oocytes expressing P2X4WT or P2X4mCherryIN as a function of the quantity of injected cDNAs. Recordings were performed the same day (2 or 3 days) postnuclear injection. Error bars represent s.e.m., the number of cells is indicated in parentheses,  $**p < 0.01$ ,  $***p < 0.001$ , one-way ANOVA and Tukey's post hoc test. Blockade of P2X4 internalization induced an approximately sevenfold increase in ATP current amplitudes. **c** Specific detection by western blots of total proteins from oocytes expressing P2X4WT (70 kDa) or P2X4mCherryIN (100 kDa) with anti-P2X4 or anti-RFP antibodies, respectively. **d** Representative immunoblots of total and surface biotinylated proteins from oocytes expressing P2X4WT (WT) or P2X4mCherryIN (mCherryIN) using anti-P2X4 or anti-RFP antibodies. Bars represent mean  $\pm$  s.e.m. of the surface/total ratio of P2X4WT (gray bars,  $4.73 \pm 1.64\%$ ,  $n = 5$ ) and P2X4mCherryIN (red bars,  $27.05 \pm 6.2\%$ ,  $n = 3$ ). The number of independent experiments is indicated in parentheses,  $*p < 0.05$ , unpaired *t*-test. **e** Confocal overlay images of hippocampal neurons transfected with extracellular HA-tagged P2X4WT or HA-P2X4mCherryIN revealed a strong increase in surface P2X4 in neurons expressing P2X4mCherryIN vs. P2X4 WT. Surface P2X4 was revealed by labeling living cells with anti-HA antibodies (green). Total P2X4 was detected after fixation, permeabilization, and staining with anti-P2X4 antibody (red) in P2X4 WT cells or by mCherry fluorescence (red) in P2X4mCherryIN cells. Scale bars, 20  $\mu$ m. **f** Mean fluorescence intensity of surface HA-P2X4WT and HA-P2X4mCherryIN illustrated in **e** and in Supplementary Fig. S1. Error bars, s.e.m., the number of cells is indicated in parentheses,  $***p < 0.001$ , unpaired Mann-Whitney test. **g, h** Enlarged image of a dendrite, showing surface clustering of HA-P2X4mCherryIN. Postsynaptic regions are indicated by detection of Homer 1c (blue). Scale bar, 5  $\mu$ m. Overall, 42% of clusters are localized in the vicinity of excitatory glutamatergic synapses. **g** Quantification of the size, fluorescence intensity, and density of clusters at extrasynaptic site and in the vicinity of glutamatergic synapses showing P2X4 form larger clusters near synapses. Error bars: s.e.m., two-way ANOVA and Tukey's post hoc test, interaction  $F(2, 341) = 11.38$ ;  $***p < 0.001$ . **i** Epifluorescence images of hippocampal neurons transfected with P2X4WT or P2X4mCherryIN revealed the strong increase of surface P2X4mCherryIN compared with P2X4WT. Surface P2X4WT and P2X4mCherryIN were revealed on living cells with Nodu-246 antibody (green) recognizing the native extracellular domain of P2X4. Total P2X4WT or P2X4mCherryIN was detected after fixation and permeabilization with anti-P2X4 antibodies (red) or directly by the red fluorescence of mCherry protein, respectively. Scale bar, 10  $\mu$ m.

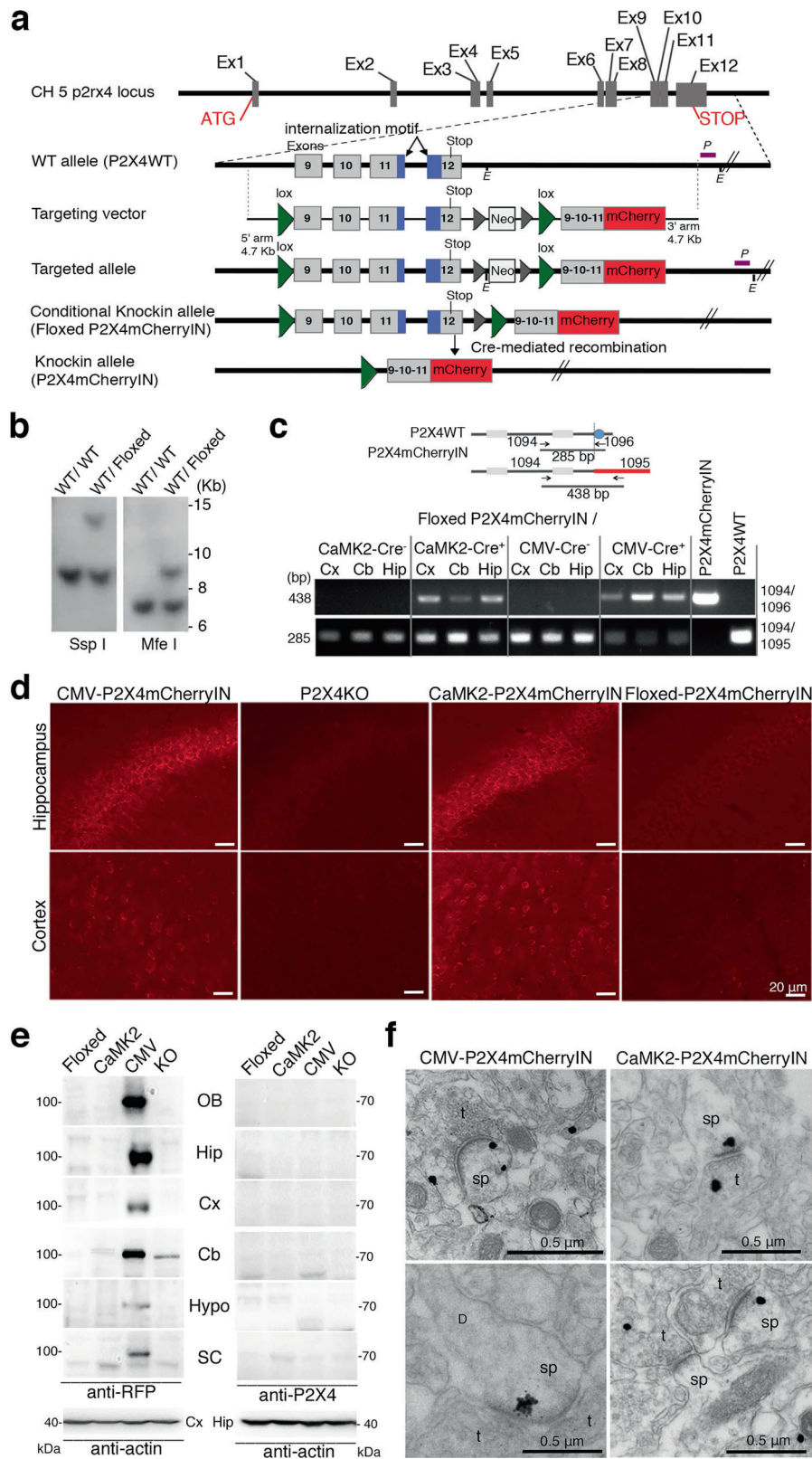
146 protein ratio showed that P2X4mCherryIN is more effectively  
147 translocated to the surface than P2X4WT in *Xenopus*  
148 oocytes (Fig. 1d,  $p < 0.05$ ).

149 We next transfected hippocampal neurons and Cos cells  
150 (Fig. 1e–h and Supplementary Fig. S1a–d) with extra-  
151 cellularly tagged HA-P2X4WT and HA-P2X4mCherryIN  
152 to visualize surface P2X4 on living cells using anti-HA

antibodies. Total HA-P2X4 was revealed after cell permeabilization using anti-P2X4 antibodies while the endogenous fluorescence of mCherry fused to P2X4 allowed for direct visualization. HA-P2X4WT is weakly expressed at the surface and is found mainly in intracellular puncta restricted to the soma and proximal dendrites of neurons [27]. In contrast, HA-P2X4mCherryIN was ~10 times more expressed at the surface of neurons. Surface P2X4mCherryIN puncta are uniformly distributed at the surface including distal dendrites. Co-staining with the postsynaptic marker Homer-1c-GFP revealed that surface P2X4mCherryIN are equally distributed in small extrasynaptic clusters and in larger clusters juxtaposed to synapses (Fig. 1g, h and Supplementary Fig. S1d). Finally, we confirmed the predominant intracellular localization of untagged P2X4WT in mouse transfected hippocampal neurons using Nodu-246, a rat monoclonal antibody recognizing the native extracellular domain of mouse P2X4 [52], whereas P2X4mCherryIN is highly and uniformly distributed at the cell surface (Fig. 1i).

## 172 Generation of knock-in mice with noninternalized 173 P2X4mCherryIN and expression in the brain

174 We generated the conditional Floxed P2X4mCherryIN  
175 knock-in mice (Floxed) by homologous recombination  
176 using a targeting vector (see Fig. 2a) designed to flox the  
177 last four exons (exons 9 to 12) of *P2rx4* allele (P2X4  
178 internalization motif being located on exons 11 and 12) and  
179 followed by the insertion of a DNA fragment corresponding  
180 to the fusion of exons 9, 10, and partially 11 with mCherry  
181 cDNA. We next generated CMVCre<sup>+</sup>-P2X4mCherryIN<sup>F/F</sup>  
182 (namely CMV) mice and CaMK2Cre<sup>+</sup>-P2X4mCherryIN<sup>F/F</sup>  
183 (CaMK2) mice by breeding Floxed mice with mice either  
184 expressing the Cre recombinase under the cytomegalovirus  
185 (CMV-Cre) or the calmodulin kinase 2 (CaMK2-Cre) promoter  
186 (Supplementary Fig. S2). Cre-dependent excision of  
187 Floxed P2X4mCherryIN allele would lead to the replacement  
188 of P2X4WT by noninternalized P2X4mCherryIN. It is  
189 important to note that excised *p2rx4* gene remains under the  
190 control of its own promoter, thus P2X4mCherryIN will  
191 replace P2X4WT only in cells expressing natively P2X4  
192 without altering its distribution pattern or its expression  
193 level. In CMV mice, where a Cre-dependent excision  
194 occurs in all cells, P2X4mCherryIN would replace  
195 P2X4WT in all cells natively expressing P2X4 throughout  
196 the body. In CaMK2 mice, substitution of P2X4WT by  
197 P2X4mCherryIN is expected to be restricted to excitatory  
198 forebrain neurons natively expressing P2X4, while other  
199 P2X4 expressing cells such as glial cells and other neuronal  
200 types express P2X4WT. Homozygous Floxed, CMV and  
201 CaMK2 mice were used in all the following experiments  
202 and were viable, normal in size or weight reproduced



203 normally and displayed no obvious physical or behavioral  
204 abnormalities (see Supplementary information).

Reverse transcription (RT)-PCR in different brain 205  
regions from the different mice showed that Floxed mice 206

**Fig. 2** Generation of conditional P2X4mCherryIN knock-in mice and P2X4 expression in CMV-Cre or CaMK2-Cre P2X4mCherryIN knock-in mice. **a** Schematic diagram of the mouse *P2xr4* gene and targeting vector strategy used to generate Floxed P2X4mCherryIN knock-in mice by homologous recombination (Floxed). By breeding Floxed P2X4mCherryIN with CMV-Cre mice or CaMK2-Cre mice, we generated constitutive CMVCre-P2X4mCherryIN (CMV) and CaMK2Cre-P2X4mCherryIN (CaMK2) to obtain a gain-of-function of P2X4 in all cells or in excitatory forebrain neurons natively expressing P2X4, respectively. **b** Southern blot of genomic DNA of WT and targeted allele (Floxed) using external probe (P) after digestion by *MfeI* or *SspI* enzyme (E) indicated in **a**. **c** Expression of P2X4WT and P2X4mCherryIN mRNAs by RT-PCR in cortex (Cx), cerebellum (Cb), and hippocampus (Hip) brain regions from Floxed P2X4mCherryIN, CMVCre<sup>+</sup>/Floxed P2X4mCherryIN (CMV) and CaMK2Cre<sup>+</sup>/Floxed P2X4mCherryIN (CaMK2) mice. **d–f** Protein expression of P2X4mCherryIN in the mouse brain revealed using anti-RFP antibodies recognizing mCherry protein. **d** Brain sections immunostained with anti-RFP antibodies show P2X4mCherryIN expression in the hippocampus and cortex of CMVCre-P2X4mCherryIN and CaMK2Cre-P2X4mCherryIN while no signal is visible in Floxed P2X4mCherryIN and P2X4 Knockout (KO) mice (see also Supplementary Fig. S3). Scale bar, 20  $\mu$ m. **e** Western blotting of total proteins extracted from distinct CNS regions isolated from CMV-P2X4mCherryIN (CMV), CaMK2-P2X4mCherryIN (CaMK2), Floxed P2X4mCherryIN, and P2X4KO mice revealed with anti-RFP or anti-P2X4 antibodies. Anti-tubulin antibody was used as a loading control. OB olfactory bulb, Hip hippocampus, Cx cortex, Cb cerebellum, Hypo hypothalamus, SC spinal cord. **f** Electron microscopy images showing preembedding anti-RFP immunostaining in CA1 region of the hippocampus or cortex from CMV-P2X4mCherryIN and CaMK2-P2X4mCherryIN mice (see also Supplementary Fig. S3). Staining is close to the plasma membrane of pre- and post-synaptic specializations of excitatory asymmetric synapses (top). Examples of spines where P2X4mCherryIN is detected only at the postsynapse, mainly located at the edge of the postsynaptic density. t presynaptic, sp spine. Scale bar, 0.5  $\mu$ m.

solely expressed P2X4WT mRNA while CMV mice only expressed P2X4mCherryIN mRNA (Fig. 2c). As expected, CaMK2 mice expressed both WT and knock-in mRNAs since only a subset of P2X4 expressing cells (forebrain excitatory neurons) replace P2X4WT by P2X4mCherryIN. Next, we tested P2X4mCherryIN expression in the brain on a protein level (Fig. 2d–f). The sparse expression of P2X4 throughout the brain observed in previous works [3, 53] was recently confirmed using tdTomato *p2xr4* reporter mice in which the detection of cytosolic tdTomato-expressing cells required the use of anti-tdTomato antibodies [15]. Not surprisingly, endogenous fluorescence of mCherry fused to P2X4 was not directly visible on brain slices of the different knock-in mice but could be visualized using anti-RFP antibodies. P2X4mCherryIN was detected in the pyramidal neuron layer of the hippocampus and in the soma of neurons throughout the cortex [3, 15] in both CMV and CaMK2, but not in Floxed or P2X4 knockout (P2X4KO) mice (Fig. 2d). In addition, we confirmed the abundant expression of P2X4mCherryIN in the epithelial glomerular layer of the olfactory bulb [15, 54], as well as a moderate

presence in cerebellar Purkinje cells [3, 15] of CMV mice but not of CaMK2 mice, as expected. These results showed that P2X4mCherryIN distribution in CMV mice is similar to that of P2X4 in WT mice [15] and the restricted detection of P2X4mCherryIN in forebrain neurons in CaMK2 mice confirmed the specificity of Cre-dependent excision. (Supplementary Fig. S3a–b). The detection of a 100 kDa band with anti-RFP antibodies in western blots of total proteins from different brain regions confirmed the substitution of P2X4WT by P2X4mCherryIN in CMV mice (Fig. 2e). The absence of detection of P2X4mCherryIN in CaMK2 mice indicated that the replacement of P2X4WT by P2X4mCherryIN is more widespread in the CMV than in CaMK2 mice, as expected. Moreover, the absence of detection of P2X4WT in Floxed or CaMK2 mice with anti-P2X4 confirmed the sparse P2X4 expression in the brain tissues (Fig. 2e).

E.M. of anti-RFP labeling in hippocampal CA1 region or cortex revealed that P2X4mCherryIN was present at post-synaptic sites of excitatory synapses, preferentially at the edge of the postsynaptic density (Fig. 2f). At some asymmetric excitatory synapses, P2X4mCherryIN was located at both pre- and post-synaptic sites (Fig. 2f) and also found intracellularly in association with the endoplasmic reticulum membranes or occasionally with mitochondria (Supplementary Fig. S3c). This suggests that replacement of P2X4WT by P2X4mCherryIN does not alter its subcellular distribution [3]. The identification of symmetric synapses on morphological criteria being difficult, the presence of P2X4 at GABAergic synapses was not confirmed in CMV mice. In contrast, E.M. analysis revealed the presence of P2X4mCherryIN in astrocytes of CMV mice in the astrocyte end-feet encircling endothelial cells (Supplementary Fig. S3d).

### Endogenous P2X4mCherryIN fluorescence is directly observable in macrophages or after LPS-induced de novo expression in microglia of CMV mice

In mice, de novo P2X4 expression was observed in spinal microglia after nerve injury or in the brain after intracerebral lipopolysaccharide (LPS) injection in tdTomato *P2xr4* reporter mice [15, 38, 39, 41, 55]. We performed in vivo LPS microinjections into the hippocampus of CMV, CaMK2, Floxed, and P2X4KO mice and examined P2X4mCherryIN fluorescence (Fig. 3 and Supplementary Fig. S4). In control saline-injected mice, no endogenous mCherry fluorescence was visible in the hippocampus of all mouse genotypes and only a faint staining was revealed for the microglial marker Iba1 (Fig. 3a). In contrast, a strong increase in Iba1 staining was detected in all LPS-injected mouse lines attesting the microglial activation (Fig. 3a, b and Supplementary Fig. S4). Remarkably, endogenous

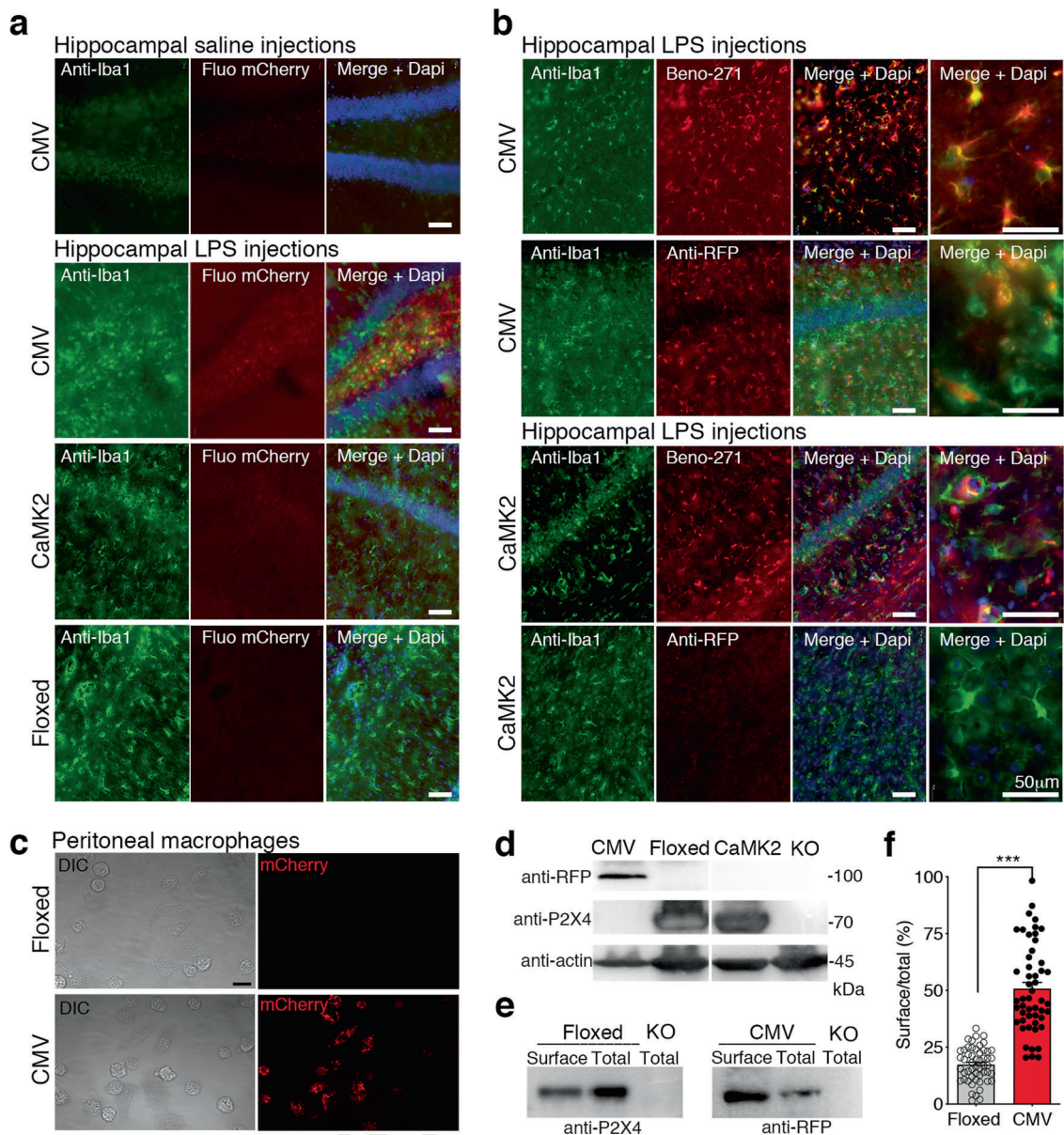


**Fig. 3 Endogenous P2X4mCherryIN fluorescence in hippocampal microglia after LPS-induced de novo P2X4 expression and in peritoneal macrophages from CMV-P2X4mCherryIN mice.** **a** Representative immunohistochemistry images of Iba1 and endogenous fluorescence of P2X4 mCherryIN (top, left) from the hippocampal region of the different mice injected with saline or 4  $\mu$ g LPS on each side (see also Supplementary Fig. S4). The mCherry fluorescence increased in Iba1-positive cells after LPS specifically in CMV mice. **b** Immunodetection of P2X4mCherryIN using Beno-271 antibodies (a camelid nanobody directed against the extracellular domain of native P2X4) and anti-RFP antibodies from CMV or CaMK2 mice after LPS injections. An enlarged overlay reveals that the increase of P2X4mCherryIN is detected in Iba1-positive microglia cells by both antibodies in CMV mice while such increase is observed only with Beno-271 in CaMK2 mice. Scale Bar, 50  $\mu$ m. **c** Endogenous P2X4mCherryIN fluorescence of macrophages isolated from the peritoneal cavity of Floxed and CMV mice. Differential interference contrast (DIC) and red fluorescence images reveal the P2X4mCherryIN exclusively in CMV mice. Scale bar, 20  $\mu$ m. **d** Western blotting

of total proteins from macrophages of CMV, CaMK2, Floxed, and P2X4KO mice using anti-RFP and anti-P2X4 revealed that P2X4WT is substituted by P2X4mCherryIN in macrophages of CMV mice only. P2X4mCherryIN is not detected by anti-P2X4 directed against the C-terminal of P2X4. Antiactin antibody was used as loading control. **e, f** Surface P2X4 expression is increased in CMV mouse peritoneal macrophages. Representative immunoblots of total and biotinylated surface proteins from peritoneal macrophages isolated from Floxed and CMV mice revealed with anti-P2X4 and anti-RFP antibodies, respectively. As in **d**, total proteins of P2X4KO macrophages were used as a negative control. **f** Quantification of surface/total expression of P2X4WT and P2X4mCherryIN in macrophages shown representatively in **e**. Bars represent mean  $\pm$  s.e.m. of the surface/total ratio of P2X4WT (Gray bar,  $17.36 \pm 1.03\%$ ,  $n = 53$ ) in Floxed mice and P2X4mCherryIN in CMV mice (red bar,  $50.79 \pm 2.71\%$ ,  $n = 51$ ) and show that P2X4 surface expression is strongly increased in cells expressing P2X4mCherryIN mice compared with those expressing P2X4WT. The number of independent experiments is indicated by clear and black circles. \*\*\*  $P < 0.001$ , unpaired  $t$ -test.



279 fluorescence of P2X4mCherryIN was directly visible and  
 280 colocalized with Iba1 in CMV mice, but not in Floxed or  
 281 CaMK2 mice. Anti-RFP confirmed the abundant and spe-  
 282 cific P2X4mCherryIN expression in Iba1-positive cells  
 283 solely in LPS-treated CMV mice. Notably, using Beno-271,  
 284 a camelid nanobody recognizing the extracellular domain of  
 285 mouse P2X4 [52], we showed increased P2X4 surface  
 286 expression in microglia of CMV, CaMK2, and Floxed but  
 287 not of P2X4KO mice (Fig. 3b and Supplementary Fig. S4).  
 288 These results validate the cellular specificity of the Cre-  
 289 mediated excision in both knock-in mice and show that de  
 290 novo expression of P2X4 induced by LPS can be directly  
 291 monitored by the visualization of the fluorescence of  
 292 mCherry fused to P2X4.

293 P2X4 has been shown to be highly expressed in mac-  
 294 rophages [41]. Endogenous mCherry fluorescence was  
 295 directly visualized in freshly isolated peritoneal macro-  
 296 phages from CMV mice (Fig. 3c), the only knock-in line  
 297 expressing P2X4mCherryIN receptors in macrophages as  
 298 confirmed by western blots of macrophages isolated from  
 299 CMV, CaMK2, Floxed, and P2X4KO mice (Fig. 3d). To  
 300 assess surface/total ratio of P2X4 and P2X4mCherryIN by  
 301 western blot analysis, biotinylation assays were performed  
 302 using macrophages in suspension. Our results showed that  
 303 the number of surface P2X4mCherryIN is significantly  
 304 higher in CMV (Fig. 3e, f) than in Floxed mice expressing  
 305 P2X4WT, demonstrating that the substitution of P2X4 by  
 306 P2X4mCherryIN leads to an increase in surface P2X4  
 307 density in macrophages from CMV mice.

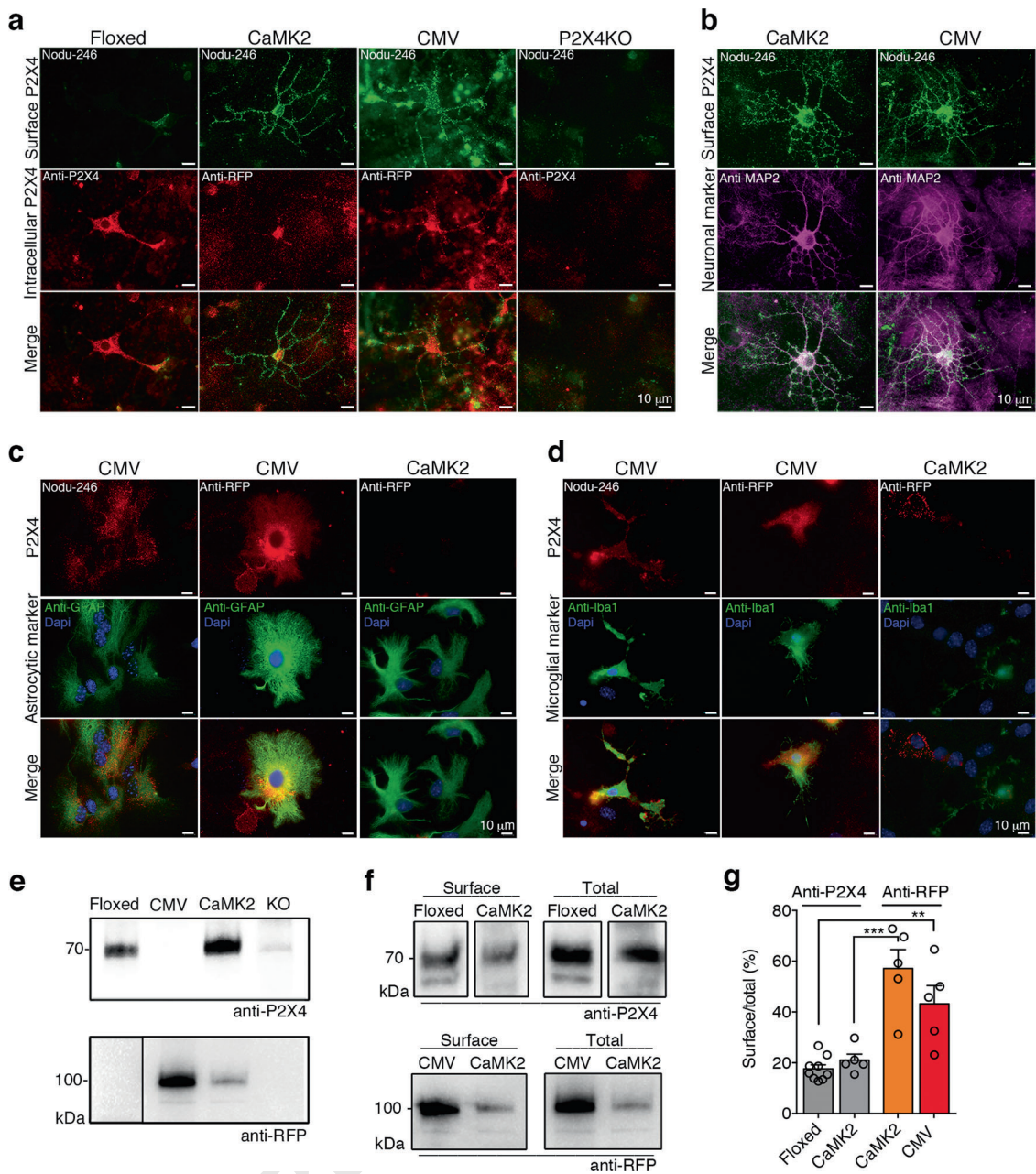
### 308 **P2X4mCherryIN is differentially upregulated at the** 309 **surface of neurons and glia in CMV and CaMK2 mice**

310 To demonstrate surface upregulation of P2X4mCherryIN in  
 311 the CNS, we performed immunofluorescence experiments  
 312 using hippocampal cultures from pups of both CMV,  
 313 CaMK2 Floxed, or P2X4KO mice. We showed the distri-  
 314 bution of surface vs. intracellular P2X4 using antibodies  
 315 targeting either the native extracellular domain of P2X4  
 316 (Nodu-246), or against the intracellular C-tail of either  
 317 P2X4WT (anti-P2X4) or P2X4mCherryIN (anti-RFP,  
 318 Fig. 4). In the Floxed mice, most P2X4WT was detected  
 319 intracellularly (Fig. 4a) as described previously [27, 28, 34].  
 320 In contrast, in both CMV and CaMK2 cells, a strong surface  
 321 staining was detected using Nodu-246, as well as the pre-  
 322 sence of RFP labeling, indicating the high density of  
 323 P2X4mCherryIN on the surface of these hippocampal cells  
 324 (Fig. 4a). In cells from P2X4KO mice, no P2X4 was  
 325 detected on the cell surface or intracellular (Fig. 4a). Anti-  
 326 MAP2 antibodies revealed the specific expression of  
 327 P2X4mCherryIN in neurons in both CMV and CaMK2  
 328 transgenic lines (Fig. 4b and Supplementary Fig. S5a).  
 329 Using antibodies against astrocytic GFAP and microglial

Iba1 markers combined with Nodu-246 and anti-RFP, 330  
 revealed the presence of surface P2X4mCherryIN in 331  
 microglia and astrocytes from CMV, but not CaMK2 mice 332  
 (Fig. 4c, d and Supplementary Fig. S5b). Consistently, 333  
 western blotting of proteins extracted from hippocampal 334  
 cultures of the different knock-in lines allowed the identi- 335  
 fication of P2X4mCherryIN proteins in the CMV and 336  
 CaMK2 exclusively, whereas P2X4WT was detected in 337  
 Floxed and CaMK2 hippocampal cells (Fig. 4e). Next, we 338  
 examined surface and total P2X4 levels using either anti- 339  
 P2X4 or anti-RFP antibodies by biotinylation assays and 340  
 western blotting of hippocampal cells from the different 341  
 transgenic mice. Quantification of immunoblots (Fig. 4f) 342  
 clearly indicates that P2X4WT in Floxed and CaMK2 mice 343  
 is mainly intracellular (Fig. 4g), while the amount of 344  
 P2X4mCherryIN on the cell surface is significantly higher 345  
 in both CMV and CaMK2 cells (Fig. 4a–d). Altogether, 346  
 these results confirm that substitution of P2X4WT by 347  
 P2X4mCherryIN is restricted to excitatory neurons of 348  
 CaMK2 mice while in CMV mice, the substitution occurs in 349  
 all cells endogenously expressing P2X4 in CMV mice. In 350  
 addition, our results demonstrate that P2X4mCherryIN 351  
 expression leads to a stronger surface localization of 352  
 P2X4mCherryIN in both CMV and CaMK2 mice (Fig. 4g). 353

### 354 **Increased surface density of P2X4 alters LTP and** 355 **LTD at CA1 hippocampal synapses**

356 We next examined the impact of noninternalized 357  
 P2X4mCherryIN in hippocampal synaptic plasticity. Field 358  
 excitatory postsynaptic potential (fEPSP) were recorded in 359  
 the hippocampal CA1 region after stimulation of pre- 360  
 synaptic Schaffer collateral axons in acute brain slices from 361  
 control Floxed and both CaMK2 or CMV mice (Fig. 5a–f). 362  
 The input/output curves obtained by plotting fEPSP slopes 363  
 against the amplitude of stimulation (Fig. 5b) showed no 364  
 significant differences between slices from CMV or CaMK2 365  
 mice compared with control Floxed mice indicating that 366  
 increased P2X4 surface receptors do not disrupt basal 367  
 excitatory transmission at CA1 synapses. LTP and LTD 368  
 were then evaluated. Robust LTP was induced in slices 369  
 from Floxed mice with persistent potentiation (Fig. 5c, d). 370  
 High frequency stimulation failed to trigger a potentiation in 371  
 CaMK2 slices, while in CMV slices a potentiation was 372  
 induced, but evoked responses returned rapidly to baseline 373  
 after the induction. At 40 min post induction, LTP was 374  
 absent in slices from both CMV and CaMK2 mice (Fig. 5c, 375  
 d). Increased surface P2X4 appears to block LTD as well 376  
 (Fig. 5e, f). LTD was induced in slices from Floxed, CMV 377  
 and CaMK2 mice but a significant persistent synaptic 378  
 depression was recorded solely in Floxed mice only 379  
 (Fig. 5e, f). LTD from CMV and CaMK2 slices was not 380  
 significantly different from baseline. Altogether, these



381 results demonstrate that increased surface P2X4 blocks LTP  
 382 and alters LTD at hippocampal CA1 synapses. Moreover,  
 383 the effects are more pronounced when surface P2X4 is  
 384 increased exclusively in forebrain excitatory neurons.

385 **Increased surface density of P2X4 in forebrain**  
 386 **neurons alters anxiety and memory functions**

387 Next, the impact of noninternalized P2X4mCherryIN  
 388 expression on the behavior of the different transgenic mice  
 389 was then examined using a battery of tests (Fig. 5g–p and  
 390 Supplementary Fig. S6). First, potential changes in their  
 391 general activity were assessed during open field exploration

(Fig. 5g–i). Floxed, CaMK2, and CMV mice showed 392  
 similar velocity and total distance traveled in the arena, 393  
 indicating that increased surface P2X4 does not modulate 394  
 basal locomotor activity (Fig. 5g, h and Supplementary 395  
 Fig. S6b). Interestingly, CaMK2 mice spent significantly 396  
 more times in the central zone (red area) compared with the 397  
 other groups of mice (Fig. 5i), suggesting that increased 398  
 surface P2X4 density may reduce anxiety-like behavior. 399  
 Neophobia-related anxiety was additionally examined by 400  
 placing a novel object in the center of the arena (Fig. 5j–l; 401  
 [56]). The latency to first exploring the novel object was 402  
 slightly lower for CaMK2 than for CMV and Floxed mice 403  
 but this difference failed to reach significance (Fig. 5k). 404

◀ **Fig. 4 Surface P2X4mCherryIN expression is increased in hippocampal neurons of CaMK2 or CMV mice as well as in glial cells of CMV mice.** **a** Representative images of surface and total P2X4WT and/or P2X4mCherryIN in Floxed, CMV, and CaMK2 primary hippocampal cell cultures reveal that surface P2X4mCherryIN is strongly increased compared with P2X4WT. Extracellular surface P2X4 and P2X4mCherryIN are visualized using Nodu-246 (green) antibodies. Intracellular P2X4WT is revealed by anti-P2X4 antibodies (red) in Floxed and P2X4KO mice while intracellular P2X4mCherryIN is revealed using anti-RFP antibodies (red) from CaMK2 and CMV mice. Staining was performed at 21 *div*. Scale bars, 10  $\mu$ m. **b** High density of surface P2X4mCherryIN using Nodu-246 (green) is detected in CaMK2 and CMV neurons identified using neuronal MAP2 marker (magenta). Surface P2X4WT is almost absent in Floxed mice and not detected in P2X4KO neurons (see Supplementary Fig. S5). **c, d** P2X4mCherryIN is expressed only in astrocytes and microglia of CMV mice solely. **c** Surface and total P2X4mCherryIN revealed using Nodu-246 and anti-RFP antibodies (red) respectively, in GFAP-positive astrocytes (green) from seven *div* primary hippocampal CMV cells. Nuclear marker DAPI is shown in blue. **d** Surface and total P2X4mCherryIN using Nodu-246 or anti-RFP antibodies (red), respectively, in microglia stained using anti-Iba1 antibodies (green) from 21 *div* primary hippocampal cells from CMV mice. Nuclear marker DAPI is shown in blue. **e** Western blotting of total proteins from primary hippocampal cells from Floxed, CMV, CaMK2, and P2X4KO mice using anti-RFP and anti-P2X4 antibodies reveal P2X4mCherryIN specifically in CMV and CaMK2 mice while P2X4WT is detected in CaMK2 and Floxed mice. **f** Representative immunoblots of total and biotinylated surface proteins from primary hippocampal cells isolated from Floxed, CMV, and CaMK2 mice revealed with either anti-P2X4, anti-RFP or both antibodies, respectively. As in **e**, total proteins of P2X4KO macrophages were used as a negative control. **g** Quantification of surface/total P2X4WT and P2X4mCherryIN in hippocampal cells. Bars represent mean  $\pm$  s.e.m. of the surface/total ratio of P2X4WT (gray bar) in Floxed and CaMK2 mice and P2X4mCherryIN in CaMK2 (orange bar) or CMV mice (red bar) and show that P2X4 surface expression is strongly increased in cells expressing P2X4mCherryIN mice compared with those expressing P2X4WT. The number of independent experiments is indicated by circles. one-way ANOVA, and Bonferroni's post hoc test,  $F(3, 20) = 17.2$ ; \* $p < 0.05$ , \*\* $p < 0.01$ , \*\*\* $p < 0.001$ .

405 However, CaMK2 mice spent significantly more time  
406 exploring the object than Floxed or CMV mice (Fig. 5l),  
407 suggesting that anxiety is lower in these mice. To cor-  
408 roborate these findings, the three mouse lines were tested in  
409 the elevated plus maze (Fig. 5m). Compared with CMV and  
410 Floxed mice, CaMK2 mice spent a greater proportion of  
411 time in the open arms of the maze, confirming their  
412 anxiolytic phenotype. These results indicate that neuronal  
413 P2X4 is involved in the regulation of anxiety-like behavior,  
414 with an increased number of P2X4 on neuronal surfaces  
415 resulting in reduced anxiety.

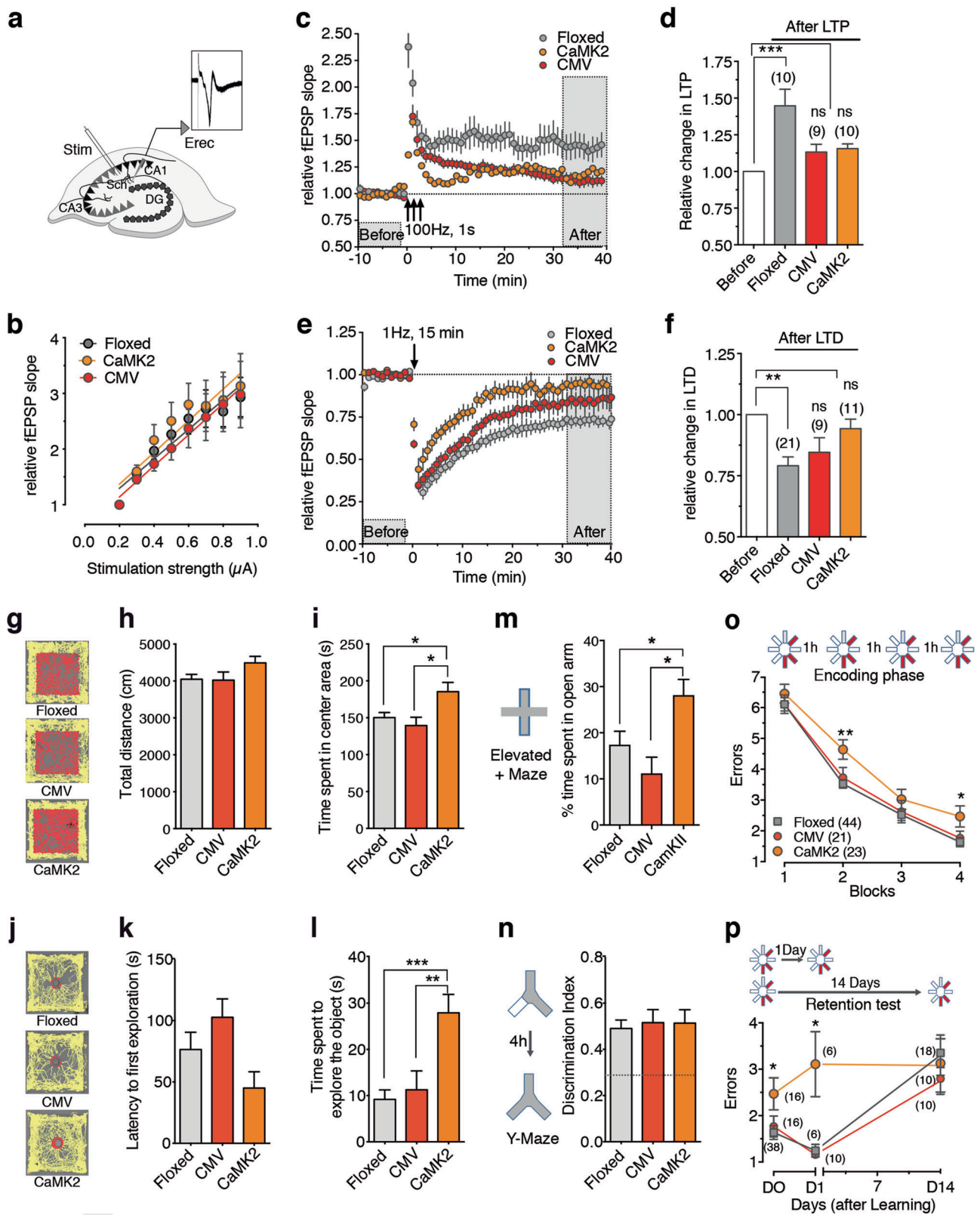
416 Spatial recognition memory was then evaluated using a  
417 modified version of the Y-maze two-trial arm discrimina-  
418 tion task (Fig. 5n and Supplementary Fig. S6; [57]). After a  
419 single encoding phase of 10 min with only two accessible  
420 arms, an inter-trial interval of 4 h resulted in a robust and  
421 similar preference for the unexplored, previously inacces-  
422 sible, arm during the test phase in CMV, CaMK2, and

Floxed mice. Thus, mice from all genotypes were capable  
of processing visuo-spatial information and forming short-  
term spatial recognition memory.

423  
424  
425  
426 We next asked whether impairments in learning and  
427 memory underlie the observed synaptic plasticity deficits.  
428 We examined spatial memory in a more cognitively chal-  
429 lenging situation by submitting CMV, CaMK2, and Floxed  
430 mice to spatial discrimination tests in the eight-arm radial  
431 maze. Mice were required to locate the three constantly  
432 baited arms of the maze (Fig. 5o). To provide a rigorous  
433 control over the time course of neuronal events induced by  
434 spatial learning, we trained the mice over one single day.  
435 Reference memory training consisted of four equivalent  
436 blocks of six trials separated by a 1 h interval. Each trial  
437 started with all eight arms opened and terminated when the  
438 mouse entered the third baited arm and returned to the  
439 central platform of the maze. While the number of reference  
440 memory errors (i.e., entries into unbaited arms) decreased  
441 significantly over the four training blocks in all three mouse  
442 lines (Fig. 5o), CaMK2 mice made significantly more errors  
443 than CMV and Floxed mice (Fig. 5k,  $p = 0.0094$ ). Poorer  
444 performance of CaMK2 was particularly apparent in train-  
445 ing blocks 2 and 4 compared with Floxed and CMV mice.  
446 Subsequently recent and long-term memory were evaluated  
447 by submitting mice to retrieval testing 1 and 14 days after  
448 training completion (Fig. 5p). As expected, Floxed mice  
449 exhibited memory decay over time with an increased  
450 number of reference memory errors at day 14. A similar  
451 decay was observed in CMV mice, indicating that forgetting  
452 was unaffected in this mouse line. In contrast, the poorer  
453 performance of CaMK2 mice achieved upon training  
454 remained stable across delays and was not further exacer-  
455 bated by the passage of time. At day 14, the number of  
456 reference memory errors was elevated but similar for all  
457 three genotypes. Thus, selective expression of non-  
458 internalized P2X4mCherryIN in excitatory forebrain neu-  
459 rons translated into impaired spatial memory processing.

## 460 Discussion

461 To address pathologically increased surface P2X4 func-  
462 tions, we created a Floxed knock-in P2X4mCherryIN  
463 mouse line and generated two distinct conditional  
464 P2X4mCherryIN lines, expressing noninternalized  
465 P2X4mCherryIN either in all cells natively expressing  
466 P2X4 (CMV mice) or in excitatory forebrain neurons  
467 (CaMK2 mice), respectively. Both CMV and CaMK2  
468 P2X4mCherryIN knock-in mice were viable, reproduced  
469 normally and displayed no manifest phenotypic issues. The  
470 key finding of this study is that the increased surface density  
471 of P2X4 in forebrain excitatory neurons is a major regulator  
472 of hippocampal synaptic plasticity, learning and memory



473 and anxiety functions indicating that increased neuronal  
 474 P2X4 observed in AD models may have a key role in the  
 475 pathogenesis of AD [25].

Importantly, analysis of P2X4mCherryIN expression  
 showed that substitution of P2X4WT by P2X4mCherryIN  
 occurred in the expected brain regions in both strains. In

476  
 477  
 478

**Fig. 5 Surface increase of neuronal P2X4 impairs LTP and LTD at CA1 hippocampal synapses and alters anxiety, spatial learning, and memory.** **a** Schematic drawing of the experimental protocol and example of an fEPSP recorded from the hippocampal CA1 region (Erec). fEPSP were induced by the electrical stimulation (stim) of the Schaffer collaterals (Sch) in the CA3 area and recorded in the stratum radiatum layer in brain slices of Floxed, CaMK2, and CMV P2X4mCherryIN mice. DG dentate gyrus. **b** The relative field slope is plotted against stimulation intensity. The input/output curves for neurons in hippocampal slices from Floxed (gray circles,  $n = 7$ ), CaMK2 (orange circles,  $n = 7$ ) and CMV P2X4mCherryIN (red circles,  $n = 6$ ) mice show similar linear regression (mean  $\pm$  s.e.m., one-way ANOVA,  $F(2, 18) = 0.15$ ;  $p = 0.85$ ) indicating that basal synaptic transmission is not affected by the increase of surface P2X4 expression. **c, d** Surface P2X4 increase impairs LTP. **c** Plots of normalized fEPSP slopes recorded in CA1 over time before and after the induction of LTP. LTP was induced by three tetanic trains (100 Hz, 1 s) with a 20 sec interval) in control Floxed ( $n = 10$ ), CaMK2 ( $n = 10$ ) or CMV mice ( $n = 9$ ). **d** Bar graph summary showing the relative change of fEPSP slope 30–40 min after the induction of LTP in Floxed ( $144.7 \pm 11.3\%$  of baseline,  $n = 10$ ), CMV mice ( $113.2 \pm 5.27\%$  of baseline,  $n = 9$ ) or CaMK2 ( $115.6 \pm 3.25\%$  of baseline,  $n = 10$ ), one-way ANOVA and tuckey's post hoc test;  $F(3, 25) = 9.41$ ;  $p = 0.002$ ,  $***p < 0.001$ . Error bars: s.e.m.; the number of mice is indicated in parentheses. **e, f** Increased surface P2X4 impairs LTD. **e** Plots of normalized fEPSP slopes recorded in CA1 over the time before and after the induction of LTD with a 1 Hz, 15 min train Floxed ( $n = 21$ ), CaMK2 ( $n = 11$ ), and CMV mice ( $n = 9$ ). **f** Bar graph summary showing the relative change of fEPSP slope 30–40 min after the induction of LTD in Floxed ( $79.09 \pm 3.63\%$  of the baseline,  $n = 22$ ,  $p < 0.001$ ), CMV ( $84.58 \pm 5.97\%$  of baseline,  $n = 8$ ,  $p > 0.05$ ) and CaMK2 mice ( $94.24 \pm 3.89\%$  of baseline,  $n = 9$ ,  $p > 0.05$ ). one-way ANOVA and tuckey's post hoc test;  $F(3, 44) = 5.44$ ;  $p = 0.0028$ ,  $**p < 0.01$ ; Error bars: s.e.m.; the number of mice is indicated in parentheses. **g–i** Open field assessments of control (Floxed mice,  $n = 24$ ) and CaMK2 ( $n = 13$ ) or CMV ( $n = 12$ ) P2X4mCherryIN mice. **g** Examples of exploration trajectories (top view) in the empty arena for each type of mice. Peripheral and central activities are indicated by yellow and red traces, respectively. **h** Similar total travel distance by

each mouse line in the empty arena during 10 min was similar. **i** CaMK2 mice spent more time in the central arena compared with Floxed and CMV mice, one-way ANOVA and Bonferroni's post hoc test;  $F(2, 46) = 5.139$ ;  $p = 0.0097$ ,  $**p < 0.01$ . **j–l** One object exploration test in control (Floxed mice,  $n = 24$ ) and CaMK2 ( $n = 13$ ) or CMV ( $n = 12$ ) P2X4mCherryIN mice. **j** Examples of exploration trajectories (top view) for each type of mice. Activities far away or at proximity of the object are indicated in yellow or red, respectively. **k** Latency to first interaction with the novel object is shown for each type of mouse. One-way ANOVA and Bonferroni's post hoc test,  $F(2, 46) = 2.868$ ;  $p = 0.067$ . **l** CaMK2 mice spent more time exploring the novel object than Floxed and CMV mice. One-way ANOVA,  $F(2, 46) = 10.27$ ;  $p = 0.0002$ ;  $**p < 0.01$ ,  $***p < 0.001$ . **m** Mean percent of time spent in the open arms of the elevated plus maze for Floxed mice ( $n = 22$ ), CaMK2 ( $n = 14$ ), and CMV ( $n = 11$ ) mice. CaMK2 spent more time in the open arms, indicating reduced anxiety compared with the other mouse lines. One-way ANOVA and Bonferroni's post hoc test,  $F(2, 44) = 5.186$ ;  $p = 0.0095$ ;  $*p < 0.05$ . **n** Spatial recognition memory evaluated in the Y-maze. Floxed ( $n = 24$ ), CaMK2 ( $n = 13$ ), or CMV ( $n = 12$ ) mice were able to recognize the novel arm of the maze that was rendered accessible 4 h after encoding (one-way ANOVA,  $F(2, 46) = 0.097$ ;  $p = 0.907$ ). **o, p** Spatial learning and memory assessment using the eight-radial maze in Floxed mice (gray), CaMK2 (orange) and CMV (red) mice. The number of mice in each group is indicated in parentheses. **o** Learning occurred over one single day and consisted of four blocks of six trials separated by a 1 h interval. The location of the three constantly baited arms of the maze is indicated in red. CaMK2 mice committed more reference memory errors (visits to unbaited arms) compared with Floxed and CMV mice.  $*p < 0.05$ ,  $**p < 0.01$ . Paired two-way ANOVA and Bonferroni's post hoc test, Time effect,  $F(3, 255) = 205.3$ ,  $p < 0.0001$ . Paired two-way ANOVA, genotype effect,  $F(2, 85) = 4927$ ,  $p = 0.0094$ . **p** Retrieval testing 1 (recent) or 14 (long-term) days after initial training in the eight-arm radial maze for all three mouse lines. Performance achieved on the fourth training block (D0) is shown for comparison. The poorer performance exhibited by CaMK2 mice (higher number of errors) was not exacerbated by the passage of time.  $*p < 0.05$ , paired two-way ANOVA and Bonferroni's post hoc test, delay effect,  $F(1, 35) = 11.70$ ;  $p = 0.0016$ . All data are presented as mean  $\pm$  s.e.m.

479 CMV mice, the expression pattern of P2X4mCherryIN is  
480 consistent with what was described for WT P2X4 in the  
481 CNS, i.e., high expression in the olfactory epithelium and a  
482 sparse expression in the hippocampus, cortex, cerebellum,  
483 and spinal cord [3, 15, 53]. In addition, and in line with  
484 other findings [41, 58], P2X4mCherryIN was also found  
485 expressed in peritoneal macrophages of CMV mice. In  
486 CaMK2 mice, P2X4mCherryIN expression was mainly  
487 restricted to hippocampal and cortical regions, in line with  
488 previous reports of CaMK2 promoter selectivity [59]. The  
489 in vitro expression of P2X4mCherryIN construct revealed  
490 that the substitution of the last 11 amino acids of the C-tail  
491 of mouse P2X4 by the red fluorescent protein mCherry  
492 increases surface trafficking without altering P2X4 function  
493 and subcellular targeting [3, 27, 28, 30, 42, 43]. Indeed, in  
494 both CMV and CaMK2 knock-in mice, E.M. confirmed that  
495 P2X4mCherryIN are localized at both pre- and post-  
496 synaptic specializations in hippocampal or cortical excita-  
497 tory neurons, as expected [2, 3, 15]. Inhibitory symmetric  
498 synapses are difficult to identify based on morphology

499 criteria, thus the presence of P2X4mCherryIN at the  
500 GABAergic synapse, where P2X4 was reported to be pre-  
501 sent, remains to be shown by including specific markers  
502 [9, 10, 42]. Surface and intracellular staining on hippo-  
503 campal cultures as well as biotinylation experiments from  
504 the different knock-in mice demonstrate that substitution of  
505 P2X4WT by P2X4mCherryIN induced a significant  
506 increase in surface P2X4 in both CaMK2 and CMV neu-  
507 rons. In addition, P2X4mCherryIN was found to be present  
508 and upregulated at the surface of hippocampal microglia  
509 and astrocytes as well as macrophages of CMV mice. P2X4  
510 expression in astrocytes has been previously observed, but  
511 was debated [60]. Notably, P2X4mCherryIN was detected  
512 in hippocampal astrocytes in vitro, but was detected on  
513 brain slices by E.M. only.

514 In contrast to transfected cells overexpressing  
515 P2X4mCherryIN, direct fluorescence of P2X4mCherryIN  
516 was undetectable from brain slices and hippocampal cul-  
517 tures of both knock-in mice, preventing the direct identifi-  
518 cation and functional characterization of P2X4mCherryIN-

519 expressing cells. Fluorescence of P2X4mCherryIN was  
520 directly visible solely in isolated peritoneal macrophages of  
521 CMV mice in agreement with its high basal expression in  
522 macrophages [41]. Interestingly, following LPS injection in  
523 the hippocampus to induce microglial activation and  
524 increase de novo P2X4 expression [15], endogenous  
525 fluorescence of P2X4mCherryIN was revealed in Iba1-  
526 positive microglia exclusively in CMV mice. These results  
527 indicate that the P2X4mCherryIN fluorescence may repre-  
528 sent a unique tool to directly monitor increased P2X4  
529 expression in pathological models such as chronic pain,  
530 AD, ALS, alcohol intake, inflammation, epilepsy, ischemia,  
531 or brain trauma [14, 19, 22, 23, 25, 26, 35–38, 55, 61].

532 LTP and LTD phenomena are widely recognized as  
533 crucial molecular mechanisms underlying cognitive func-  
534 tions such as learning and memory [62]. Although activa-  
535 tion of P2X receptors by glial ATP was recently shown to  
536 directly modulate glutamatergic synaptic strength [10], P2X  
537 receptors exert modulatory actions exclusively during  
538 activity-dependent plasticity at central synapses and do not  
539 influence basal synaptic transmission [17, 18, 63]. Previous  
540 studies have shown P2X4 modulating hippocampal LTP via  
541 N-methyl-D-aspartate receptor receptors (NMDAR), how-  
542 ever these findings remained controversial. The first work  
543 using P2X4KO mice revealed that LTP in CA1 neurons was  
544 slightly reduced compared with WT mice and that potentia-  
545 tion of P2X4 by ivermectin enhanced LTP only in WT  
546 mice [17]. Results suggested that P2X4 may enhance the  
547 content of NR2B subunits in synaptic NMDARs [63]. In  
548 contrast, an other study showed that the pharmacological  
549 blockade of P2X4 facilitated the induction of NMDAR-  
550 dependent LTP indicating an inhibitory impact of P2X4  
551 [18, 64]. Furthermore, increased P2X4 expression was  
552 reported in AD models [25] suggesting that P2X4 might  
553 also contribute to synaptic dysfunction and memory deficits.  
554 Field potential recordings show that P2X4mCherryIN  
555 expression does not change the basal excitatory transmis-  
556 sion at CA1 synapses but causes impairments in both LTP  
557 and LTD in agreement with a negative impact of P2X4 on  
558 synaptic plasticity. Surprisingly, but in full agreement with  
559 our behavioral results, these deficits were stronger in  
560 CaMK2 than in CMV mice. Impaired LTP observed in  
561 CaMK2 mice occurred immediately suggesting a deficit of  
562 LTP induction. In contrast, in CMV mice, LTP was induced  
563 but progressively returned to baseline, rather indicating a  
564 deficit in LTP maintenance. Since basal excitation mediated  
565 by  $\alpha$ -amino-3-hydroxy-5-methyl-4-isoxazolepropionic acid  
566 receptor (AMPA) is unchanged, and LTD or LTP in  
567 hippocampal CA1 neurons are mainly initiated post  
568 synaptically by NMDAR [62], our results suggest that  
569 increased P2X4 in CA1 neurons might alter NMDAR  
570 function. P2X4 is highly permeable to calcium and can  
571 mediate a strong calcium influx at the resting membrane

572 potential that may induce NMDAR inactivation [64]. P2X4  
573 interacts also dynamically with various other ligand-gated  
574 ion channels such as GABA<sub>A</sub> [10, 42, 65] and may lead to  
575 NMDAR inhibition by similar crosstalk.

576 Behavioral phenotyping of the CMV mice did not reveal  
577 any overt alterations. In contrast, CaMK2 mice exhibited a  
578 significant decrease in anxiety-like behaviors and impaired  
579 spatial learning and memory functions. No change in  
580 locomotor, anxiety-like or cognitive functions were pre-  
581 viously observed in P2X4KO mice [66]. Together, these  
582 results suggest that, in contrast to the basal state, increased  
583 surface P2X4 density observed in neurons in pathological  
584 situations such as in AD [25] might play essential roles in  
585 the regulation of synaptic plasticity and behavior such as  
586 anxiety and learning and memory.

587 The absence of a phenotype of the CMV mice, although  
588 in agreement with the weaker effects on the synaptic plas-  
589 ticity of CMV compared with CaMK2 mice, is intriguing  
590 since substitution of P2X4WT by P2X4mCherryIN in all  
591 cells natively expressing P2X4 was expected to have more  
592 pronounced effects than specific P2X4mCherryIN expres-  
593 sion solely in forebrain excitatory neurons. However, this  
594 could be explained by temporal differences between CMV  
595 and CaMK2 promoter activation. CMV is a ubiquitous early  
596 gene promoter leading to the genetic excision of Floxed  
597 P2X4mCherryIN in the germ-line and consequently from  
598 the beginning of the embryonic development while the  
599 CaMK2 promoter is considered as an adult promoter with  
600 postnatal activity reaching its maximum around the third  
601 postnatal week [67]. Expression of P2X4mCherryIN in all  
602 cells natively expressing P2X4 during the developmental  
603 period and thereafter may have deleterious effects leading to  
604 developmental compensations. Another possibility is that  
605 the expression of P2X4mCherryIN in CMV mice in other  
606 types of neurons along with expression in glial cells may  
607 counterbalance the effect of its increased surface density  
608 specifically in excitatory neurons. Indeed, increased P2X4  
609 expression in spinal cord microglia during neuropathic  
610 conditions triggers the release of BDNF by microglia  
611 resulting in neuronal hyperexcitability [39, 40]. In addition,  
612 microglia and BDNF have been shown to influence synaptic  
613 plasticity and learning in the brain [68]. These results sug-  
614 gest that increased surface P2X4 in microglia of CMV mice  
615 may promote synaptic plasticity and counterbalance the  
616 negative impact of an increase of surface P2X4 specifically  
617 in excitatory neurons of CaMK2 mice.

618 P2X4 is present in multiple cell types in the peripheral or  
619 CNS and in various epithelial, endothelial, or immune cells.  
620 After injury and during inflammation and cell damage, high  
621 levels of ATP are released and P2X4 is strongly upregulated  
622 on cell surfaces. This upregulation seems to orchestrate key  
623 events during neurodegenerative diseases, neuropathic and  
624 inflammatory pain, ischemia-induced inflammation, alcohol

625 intake, airways inflammation in asthma, rheumatoid arthritis  
626 or postsurgical liver regeneration (see for review [14]).

627 These novel conditional knock-in mice defective for  
628 P2X4 internalization provide a valuable tool which will  
629 allow to further decipher the role of upregulated P2X4 state  
630 not only in the context of neurological diseases, but also of  
631 peripheral inflammation, infection as well as in lung, car-  
632 diac or liver functions [69–73].

633 **Acknowledgements** We thank G. Dabee for the production of all  
634 transgenic mice at the animal facility, H. Orignac for help with  
635 *Xenopus* facilities and E. Normand for stereotaxic injection. We thank  
636 the Mouse Clinical Institute (Institut Clinique de la Souris, MCI/ICS)  
637 in the Genetic Engineering and Model Validation Department who  
638 established the mouse mutant floxed P2X4mCherryIN line. We also  
639 thank the biochemistry facility of Bordeaux Neurocampus. Electron  
640 microscopy was performed at the Bordeaux Imaging Center, a service  
641 unit of the CNRS-INSERM and Bordeaux University. This work was  
642 supported by CNRS, University of Bordeaux, a grant LabEx BRAIN  
643 ANR-10-LABX-43 to EB-G and EB, a grant from Inserm for the  
644 generation of the mouse line to EB-G, the Louise and Alan Edwards  
645 Foundation, an awarded grant from Quebec Pain Research Network  
646 (QPRN) to TD, International Ph. D program of the IdEx of Bordeaux  
647 to EB-G and PS and DFG grant SFB1328-Z02 to FK-N.

648 **Author contributions** EB, TD, KSP, AM, J-TP, ED, A-EA, ET, MR,  
649 FG, ON performed the experiments and analyzed the data. PS, BB, SL,  
650 FG, SB, ON and EB-G designed the experiments and analyzed the  
651 data. PB, EB, FK-N contributed with key reagents. EB-G conceived  
652 the knock-in mice and the study. KSP, ON, and EB-G wrote the paper.  
653 All authors commented the paper.

## 654 Compliance with ethical standards

655 **Conflict of interest** The authors declare they have no conflict of  
656 interest.

657 **Ethical approval** All experimental procedures complied with official  
658 European guidelines for the care and use of laboratory animals  
659 (Directive 2010/63/UE).

660 **Publisher's note** Springer Nature remains neutral with regard to  
661 jurisdictional claims in published maps and institutional affiliations.

## 662 References

- 663 1. Khakh BS, North RA. Neuromodulation by extracellular ATP and  
664 P2X receptors in the CNS. *Neuron*. 2012;76:51–69.
- 665 2. Rodrigues RJ, Almeida T, Richardson PJ, Oliveira CR, Cunha  
666 RA. Dual presynaptic control by ATP of glutamate release via  
667 facilitatory P2X1, P2X2/3, and P2X3 and inhibitory P2Y1, P2Y2,  
668 and/or P2Y4 receptors in the rat hippocampus. *J Neurosci*.  
669 2005;25:6286–95.
- 670 3. Rubio ME, Soto F. Distinct localization of P2X receptors at exci-  
671 tatory postsynaptic specializations. *J Neurosci*. 2001;21:641–53.
- 672 4. Kaczmarek-Hajek K, Zhang J, Kopp R, Grosche A, Rissiek B,  
673 Saul A, et al. Re-evaluation of neuronal P2X7 expression using  
674 novel mouse models and a P2X7-specific nanobody. *eLife*.  
675 2018;7:e36217.
- 676 5. Jo YH, Schlichter R. Synaptic corelease of ATP and GABA in  
677 cultured spinal neurons. *Nat Neurosci*. 1999;2:241–5.

- 678 6. Mori M, Heuss C, Gahwiler BH, Gerber U. Fast synaptic trans-  
679 mission mediated by P2X receptors in CA3 pyramidal cells of rat  
680 hippocampal slice cultures. *J Physiol*. 2001;535:115–23.
- 681 7. Gordon GR, Baimoukhametova DV, Hewitt SA, Rajapaksha WR,  
682 Fisher TE, Bains JS. Norepinephrine triggers release of glial ATP  
683 to increase postsynaptic efficacy. *Nat Neurosci*. 2005;8:1078–86.
- 684 8. Pougnet JT, Toulme E, Martinez A, Choquet D, Hosy E, Boue-  
685 Grabot E. ATP P2X receptors downregulate AMPA receptor  
686 trafficking and postsynaptic efficacy in hippocampal neurons.  
687 *Neuron*. 2014;83:417–30.
- 688 9. Lalo U, Palygin O, Rasooli-Nejad S, Andrew J, Haydon PG,  
689 Pankratov Y. Exocytosis of ATP from astrocytes modulates  
690 phasic and tonic inhibition in the neocortex. *PLoS Biol*. 2014;12:  
691 e1001747.
- 692 10. Boué-Grabot E, Pankratov Y. Modulation of central synapses by  
693 astrocyte-released ATP and postsynaptic P2X receptors. *Neural*  
694 *Plast*. 2017;2017:9454275.
- 695 11. Illes P, Verkhratsky A. Purinergic neurone-glia signalling in  
696 cognitive-related pathologies. *Neuropharmacology*. 2016;104:62–75.
- 697 12. Kawate T, Michel JC, Birdsong WT, Gouaux E. Crystal structure  
698 of the ATP-gated P2X(4) ion channel in the closed state. *Nature*.  
699 2009;460:592–8.
- 700 13. Egan TM, Khakh BS. Contribution of calcium ions to P2X  
701 channel responses. *J Neurosci*. 2004;24:3413–20.
- 702 14. Suurväli J, Boudinot P, Kanellopoulos J, Rüttel Boudinot S.  
703 P2X4: a fast and sensitive purinergic receptor. *Biomed J*.  
704 2017;40:245–56.
- 705 15. Xu J, Bernstein AM, Wong A, Lu XH, Khoja S, Yang XW, et al.  
706 P2X4 receptor reporter mice: sparse brain expression and feeding-  
707 related presynaptic facilitation in the arcuate nucleus. *J Neurosci*.  
708 2016;36:8902–20.
- 709 16. Yeung D, Kharidia R, Brown SC, Gorecki DC. Enhanced expres-  
710 sion of the P2X4 receptor in Duchenne muscular dystrophy corre-  
711 lates with macrophage invasion. *Neurobiol Dis*. 2004;15:212–20.
- 712 17. Sim JA, Chaumont S, Jo J, Ulmann L, Young MT, Cho K, et al.  
713 Altered hippocampal synaptic potentiation in P2X4 knock-out  
714 mice. *J Neurosci*. 2006;26:9006–9.
- 715 18. Pankratov Y, Lalo U, Krishtal OA, Verkhratsky A P2X receptors  
716 and synaptic plasticity. *Neuroscience*. 2008.
- 717 19. Cavaliere F, Florenzano F, Amadio S, Fusco FR, Viscomi MT,  
718 D'Ambrosi N, et al. Up-regulation of P2X2, P2X4 receptor and  
719 ischemic cell death: prevention by P2 antagonists. *Neuroscience*.  
720 2003;120:85–98.
- 721 20. Franke H, Illes P. Involvement of P2 receptors in the growth and  
722 survival of neurons in the CNS. *Pharm Ther*. 2006;109:297–324.
- 723 21. Burnstock G. Purinergic signalling and disorders of the central  
724 nervous system. *Nat Rev Drug Disco*. 2008;7:575–90.
- 725 22. Apolloni S, Montilli C, Finocchi P, Amadio S. Membrane com-  
726 partments and purinergic signalling: P2X receptors in neurodegen-  
727 erative and neuroinflammatory events. *FEBS J*. 2009;276:354–64.
- 728 23. Volonte C, Apolloni S, Parisi C, Amadio S. Purinergic contribu-  
729 tion to amyotrophic lateral sclerosis. *Neuropharmacology*. 2016;  
730 104:180–93.
- 731 24. Beggs S, Trang T, Salter MW. P2X4R+ microglia drive neuro-  
732 pathic pain. *Nat Neurosci*. 2012;15:1068–73.
- 733 25. Varma R, Chai Y, Troncoso J, Gu J, Xing H, Stojilkovic SS, et al.  
734 Amyloid-beta induces a caspase-mediated cleavage of P2X4 to  
735 promote purinotoxicity. *Neuromolecular Med*. 2009;11:63–75.
- 736 26. Casanovas A, Hernandez S, Tarabal O, Rossello J, Esquerda JE.  
737 Strong P2X4 purinergic receptor-like immunoreactivity is selec-  
738 tively associated with degenerating neurons in transgenic rodent  
739 models of amyotrophic lateral sclerosis. *J Comp Neurol*.  
740 2008;506:75–92.
- 741 27. Bobanovic LK, Royle SJ, Murrell-Lagnado RD. P2X receptor  
742 trafficking in neurons is subunit specific. *J Neurosci*. 2002;  
743 22:4814–24.

- 744 28. Royle SJ, Bobanovic LK, Murrell-Lagnado RD. Identification of a  
745 non-canonical tyrosine-based endocytic motif in an ionotropic  
746 receptor. *J Biol Chem.* 2002;277:35378–85.
- 747 29. Qureshi OS, Paramasivam A, Yu JC, Murrell-Lagnado RD.  
748 Regulation of P2X4 receptors by lysosomal targeting, glycan  
749 protection and exocytosis. *J Cell Sci.* 2007;120:3838–49.
- 750 30. Royle SJ, Qureshi OS, Bobanovic LK, Evans PR, Owen DJ,  
751 Murrell-Lagnado RD. Non-canonical YXXGPhi endocytic motifs:  
752 recognition by AP2 and preferential utilization in P2X4 receptors.  
753 *J Cell Sci.* 2005;118:3073–80.
- 754 31. Toulme E, Garcia A, Samways D, Egan TM, Carson MJ, Khakh  
755 BS. P2X4 receptors in activated C8-B4 cells of cerebellar  
756 microglial origin. *J Gen Physiol.* 2010;135:333–53.
- 757 32. Cao Q, Zhong XZ, Zou Y, Murrell-Lagnado R, Zhu MX, Dong XP.  
758 Calcium release through P2X4 activates calmodulin to promote  
759 endolysosomal membrane fusion. *J Cell Biol.* 2015;209:879–94.
- 760 33. Huang P, Zou Y, Zhong XZ, Cao Q, Zhao K, Zhu MX, et al.  
761 P2X4 forms functional ATP-activated cation channels on lyso-  
762 somal membranes regulated by luminal pH. *J Biol Chem.*  
763 2014;289:17658–67.
- 764 34. Robinson LE, Murrell-Lagnado RD. The trafficking and targeting  
765 of P2X receptors. *Front Cell Neurosci.* 2013;7:233.
- 766 35. Andries M, Van Damme P, Robberecht W, Van Den Bosch L.  
767 Ivermectin inhibits AMPA receptor-mediated excitotoxicity in  
768 cultured motor neurons and extends the life span of a transgenic  
769 mouse model of amyotrophic lateral sclerosis. *Neurobiol Dis.*  
770 2007;25:8–16.
- 771 36. Khoja S, Huynh N, Asatryan L, Jakowec MW, Davies DL.  
772 Reduced expression of purinergic P2X4 receptors increases  
773 voluntary ethanol intake in C57BL/6J mice. *Alcohol.* 2018;  
774 68:63–70.
- 775 37. Wyatt LR, Finn DA, Khoja S, Yardley MM, Asatryan L, Alkana  
776 RL, et al. Contribution of P2X4 receptors to ethanol intake in male  
777 C57BL/6 mice. *Neurochem Res.* 2014;39:1127–39.
- 778 38. Tsuda M, Shigemoto-Mogami Y, Koizumi S, Mizokoshi A,  
779 Kohsaka S, Salter MW, et al. P2X4 receptors induced in spinal  
780 microglia gate tactile allodynia after nerve injury. *Nature.*  
781 2003;424:778–83.
- 782 39. Ulmann L, Hatcher JP, Hughes JP, Chaumont S, Green PJ,  
783 Conquet F, et al. Up-regulation of P2X4 receptors in spinal  
784 microglia after peripheral nerve injury mediates BDNF release and  
785 neuropathic pain. *J Neurosci.* 2008;28:11263–8.
- 786 40. Coull JA, Beggs S, Boudreau D, Boivin D, Tsuda M, Inoue K,  
787 et al. BDNF from microglia causes the shift in neuronal anion  
788 gradient underlying neuropathic pain. *Nature.* 2005;438:1017–21.
- 789 41. Ulmann L, Hirbec H, Rassendren F. P2X4 receptors mediate  
790 PGE2 release by tissue-resident macrophages and initiate  
791 inflammatory pain. *EMBO J.* 2010;29:2290–300.
- 792 42. Jo YH, Donier E, Martinez A, Garret M, Toulme E, Boue-Grabot  
793 E. Cross-talk between P2X4 and gamma-aminobutyric acid, type  
794 A receptors determines synaptic efficacy at a central synapse. *J  
795 Biol Chem.* 2011;286:19993–20004.
- 796 43. Toulme E, Soto F, Garret M, Boue-Grabot E. Functional prop-  
797 erties of internalization-deficient P2X4 receptors reveal a novel  
798 mechanism of ligand-gated channel facilitation by ivermectin.  
799 *Mol Pharm.* 2006;69:576–87.
- 800 44. Chamma I, Heubl M, Chevy Q, Renner M, Moutkine I, Eugene E,  
801 et al. Activity-dependent regulation of the K/Cl transporter KCC2  
802 membrane diffusion, clustering, and function in hippocampal  
803 neurons. *J Neurosci.* 2013;33:15488–503.
- 804 45. Ray A, Dittel BN. Isolation of mouse peritoneal cavity cells. *J Vis  
805 Exp.* 2010.
- 806 46. Berthet A, Porras G, Doudnikoff E, Stark H, Cador M, Bezard E,  
807 et al. Pharmacological analysis demonstrates dramatic alteration of  
808 D1 dopamine receptor neuronal distribution in the rat analog of L-  
809 DOPA-induced dyskinesia. *J Neurosci.* 2009;29:4829–35.
47. Bertin E, Martinez A, Boue-Grabot E. P2X Electrophysiology and  
810 Surface Trafficking in *Xenopus* Oocytes. *Methods Mol Biol.*  
811 2020;2041:243–59.
48. Belzung C. Hippocampal mossy fibres: implication in novelty  
812 reactions or in anxiety behaviours? *Behav Brain Res.* 1992;  
813 51:149–55.
49. Renner MJ, Bennett AJ, White JC. Age and sex as factors influ-  
814 encing spontaneous exploration and object investigation by pre-  
815 adult rats (*Rattus norvegicus*). *J Comp Psychol.* 1992;106:217–27.
50. Pellow S, File SE. Anxiolytic and anxiogenic drug effects on  
816 exploratory activity in an elevated plus-maze: a novel test of  
817 anxiety in the rat. *Pharm Biochem Behav.* 1986;24:525–9.
51. Dellu F, Contarino A, Simon H, Koob GF, Gold LH. Genetic  
818 differences in response to novelty and spatial memory using a  
819 two-trial recognition task in mice. *Neurobiol Learn Mem.*  
820 2000;73:31–48.
52. Bergmann P, Garcia de Paco A, Rissiek B, Menzel S, Dubberke  
821 G, Hua J et al. Generation and characterization of specific  
822 monoclonal antibodies and Nanobodies directed against the ATP-  
823 gated channel P2X4. *Front Cell Neurosci.* in press.
53. Lê KT, Villeneuve P, Ramjaun AR, McPherson PS, Beaudet A,  
824 Seguela P. Sensory presynaptic and widespread somatodendritic  
825 immunolocalization of central ionotropic P2X ATP receptors.  
826 *Neuroscience.* 1998;83:177–90.
54. Buell G, Lewis C, Collo G, North RA, Surprenant A. An  
827 antagonist-insensitive P2X receptor expressed in epithelia and  
828 brain. *EMBO J.* 1996;15:55–62.
55. Ulmann L, Levavasseur F, Avignone E, Peyrourou R, Hirbec H,  
829 Audinat E, et al. Involvement of P2X4 receptors in hippocampal  
830 microglial activation after status epilepticus. *Glia.* 2013;  
831 61:1306–19.
56. Dulawa SC, Grandy DK, Low MJ, Paulus MP, Geyer MA.  
832 Dopamine D4 receptor-knock-out mice exhibit reduced explora-  
833 tion of novel stimuli. *J Neurosci.* 1999;19:9550–6.
57. Nicole O, Hadzibegovic S, Gajda J, Bontempi B, Bem T, Meyr-  
834 and P. Soluble amyloid beta oligomers block the learning-induced  
835 increase in hippocampal sharp wave-ripple rate and impair spatial  
836 memory formation. *Sci Rep.* 2016;6:22728.
58. Layhadi JA, Turner J, Crossman D, Fountain SJ. ATP evokes Ca  
837 (2+) responses and CXCL5 secretion via P2X4 receptor activa-  
838 tion in human monocyte-derived macrophages. *J Immunol.*  
839 2018;200:1159–68.
59. T sien JZ, Chen DF, Gerber D, Tom C, Mercer EH, Anderson DJ,  
840 et al. Subregion- and cell type-restricted gene knockout in mouse  
841 brain. *Cell.* 1996;87:1317–26.
60. Stokes L, Layhadi JA, Bibic L, Dhuna K, Fountain SJ. P2X4  
842 receptor function in the nervous system and current breakthroughs  
843 in pharmacology. *Front Pharm.* 2017;8:291.
61. Franklin KM, Asatryan L, Jakowec MW, Trudell JR, Bell RL,  
844 Davies DL. P2X4 receptors (P2X4Rs) represent a novel target for  
845 the development of drugs to prevent and/or treat alcohol use  
846 disorders. *Front Neurosci.* 2014;8:176.
62. Huganir RL, Nicoll RA. AMPARs and synaptic plasticity: the last  
847 25 years. *Neuron.* 2013;80:704–17.
63. Baxter AW, Choi SJ, Sim JA, North RA. Role of P2X4 receptors  
848 in synaptic strengthening in mouse CA1 hippocampal neurons.  
849 *Eur J Neurosci.* 2011;34:213–20.
64. Pankratov YV, Lalo UV, Krishnal OA. Role for P2X receptors in  
850 long-term potentiation. *J Neurosci.* 2002;22:8363–9.
65. Jo YH, Boue-Grabot E. Interplay between ionotropic receptors  
851 modulates inhibitory synaptic strength. *Commun Integr Biol.*  
852 2011;4:706–9.
66. Wyatt LR, Goudar SC, Khoja S, Jakowec MW, Alkana RL, Bor-  
853 tolato M et al. Sociocommunicative and sensorimotor impairments  
854 in male P2X4-deficient mice. *Neuropsychopharmacology.*  
855 2013;38:1993–2002.



- 876 67. Mayford M, Bach ME, Huang YY, Wang L, Hawkins RD, Kandel 888  
877 ER. Control of memory formation through regulated expression of 889  
878 a CaMKII transgene. *Science*. 1996;274:1678–83. 890
- 879 68. Parkhurst CN, Yang G, Ninan I, Savas JN, Yates JR 3rd, Lafaille JJ, 891  
880 et al. Microglia promote learning-dependent synapse formation 892  
881 through brain-derived neurotrophic factor. *Cell*. 2013;155:1596–609. 893
- 882 69. Hafner S, Wagner K, Weber S, Groger M, Wepler M, McCook O, 894  
883 et al. Role of the purinergic receptor P2XR4 after blunt chest 895  
884 trauma in cigarette smoke-exposed mice. *Shock*. 2017;47:193–9. 896
- 885 70. Chen H, Xia Q, Feng X, Cao F, Yu H, Song Y, et al. Effect of 897  
886 P2X4R on airway inflammation and airway remodeling in allergic  
887 airway challenge in mice. *Mol Med Rep*. 2016;13:697–704.
71. Yang T, Shen JB, Yang R, Redden J, Dodge-Kafka K, Grady J, 888  
et al. Novel protective role of endogenous cardiac myocyte P2X4 889  
receptors in heart failure. *Circ Heart Fail*. 2014;7:510–8. 890
72. Pettengill MA, Marques-da-Silva C, Avila ML, d'Arc dos Santos 891  
Oliveira S, Lam VW, Ollawa I, et al. Reversible inhibition of 892  
Chlamydia trachomatis infection in epithelial cells due to stimu- 893  
lation of P2X(4) receptors. *Infect Immun*. 2012;80:4232–8. 894
73. Gonzales E, Julien B, Serriere-Lanneau V, Nicou A, Doignon I, 895  
Lagoudakis L, et al. ATP release after partial hepatectomy reg- 896  
ulates liver regeneration in the rat. *J Hepatol*. 2010;52:54–62. 897

UNCORRECTED PROOF

Journal : 41380

Article : 641

**SPRINGER NATURE**

## Author Query Form

**Please ensure you fill out your response to the queries raised below and return this form along with your corrections**

Dear Author

During the process of typesetting your article, the following queries have arisen. Please check your typeset proof carefully against the queries listed below and mark the necessary changes either directly on the proof/online grid or in the 'Author's response' area provided below

Queries	Details Required	Author's Response
AQ1	Please check your article carefully, coordinate with any co-authors and enter all final edits clearly in the eproof, remembering to save frequently. Once corrections are submitted, we cannot routinely make further changes to the article.	
AQ2	Note that the eproof should be amended in only one browser window at any one time; otherwise changes will be overwritten.	
AQ3	Author surnames have been highlighted. Please check these carefully and adjust if the first name or surname is marked up incorrectly. Note that changes here will affect indexing of your article in public repositories such as PubMed. Also, carefully check the spelling and numbering of all author names and affiliations, and the corresponding email address(es).	
AQ4	You cannot alter accepted Supplementary Information files except for critical changes to scientific content. If you do resupply any files, please also provide a brief (but complete) list of changes. If these are not considered scientific changes, any altered Supplementary files will not be used, only the originally accepted version will be published.	
AQ5	Please provide the page range and volume number for references 18 and 45.	
AQ6	Please complete and update reference 52.	